

Modular Multi-level Converters Impedance Computation Based on Periodic Small-Signal Analysis and Vector Fitting

D. del Giudice *IEEE Student Member*, A. Brambilla *Member, IEEE*, D. Linaro *Member, IEEE*, F. Bizzarri, *Senior Member, IEEE*

Abstract—Instability and oscillation issues originating in high-voltage direct current (HVDC) systems comprising modular multilevel converters (MMCs) are gaining increasing interest in the research community. To detect such phenomena in advance, considerable effort has been devoted recently to developing MMC models for small-signal analysis. The derivation of such models is a challenging task due to the topology and complex control structure of MMCs, which results in them having a multi-frequency response. To address this issue, scholars developed methods based on dynamic phasors and harmonic state-space modelling, which, however, require extensive pen-and-paper computations. In this paper, the periodic small-signal analysis (PAC) is adopted to determine numerically several MMCs transfer functions. Such functions can be computed between any electrical circuit node or input/output port, without the need to recast the three-phase average MMC model to derive a linear equivalent one, possibly in the DQ-frame. We show how vector fitting allows converting these functions to equivalent algebraic representations, which can be profitably used to design MMCs and study their stability following some parameter changes. To showcase this feature, we exploit one of these transfer functions to detect DC-side instability in a point-to-point HVDC system.

Index Terms—Modular multilevel converters, electrical simulation, periodic small-signal analysis, small-signal impedance/admittance model, vector fitting.

I. INTRODUCTION

MODULAR multilevel converters have become the technology of choice in HVDC transmission systems thanks to their scalability to high voltages and powers, lower switching activity of the submodules (SMs) composing their legs, high voltage waveform quality, and efficiency [1]–[3]. In light of their increasing penetration in modern power systems, modular multilevel converters small-signal impedance models are crucial during the MMC design phase to identify the source of possible instability issues and oscillation phenomena [4]. The development of these models is a challenging task due to the structure of the MMC, which is more complicated than that of conventional two-level voltage source converters (VSCs) [5]. For instance, the circulating current flowing in each arm and

Davide del Giudice, Angelo Brambilla and Daniele Linaro are with Politecnico di Milano, DEIB, p.zza Leonardo da Vinci, n. 32, 20133 Milano, Italy. (e-mail: {davide.delgiudice,angelo.brambilla,daniele.linaro}@polimi.it). Federico Bizzarri is with Politecnico di Milano, DEIB, p.zza Leonardo da Vinci, n. 32, 20133 Milano, Italy and also with the Advanced Research Center on Electronic Systems for Information and Communication Technologies E. De Castro (ARCES), University of Bologna, 41026 Bologna, Italy. (e-mail: federico.bizzarri@polimi.it).

the capacitor voltage ripple of every SM in the MMC require *ad hoc* controls [6] as the steady-state harmonic content of these two variables leads to the converter having a multi-frequency response [7]. Moreover, the cross-coupling behavior of the MMC causes the interaction of its internal variables at different frequencies [8]. Hence, the elimination of higher-order harmonics demands a careful evaluation to prevent erroneous estimates. Additionally, given the non-linear switching nature of MMCs, conventional frequency scan techniques [9] (i.e., standard small-signal analysis aimed at calculating the small-signal response of a circuit in the neighborhood of an equilibrium point) cannot be used to derive MMCs small-signal impedance models, unless reduced/simplified representations are adopted.

One of the methods used to derive a small-signal model of the MMC for stability studies is based on dynamic phasors, which can be seen as an extension of the Fourier series coefficients to the case of nearly periodic systems [10]. The main advantage of using dynamic phasors, compared to a more conventional DQ transformation, lies in the fact that the obtained small-signal models are amenable to linearization and eigenvalue analysis. For instance, in [11] the authors developed a dynamic phasor model of an MMC incorporating various control strategies: the results of the small-signal eigenvalue analysis were compared to three-phase time domain simulations and found to be in good agreement. This approach was extended in several other works [12]–[15], where the authors investigated the effects of various MMC control strategies, representation frames and balanced or unbalanced system conditions on system stability and resilience to high-frequency resonance.

Another approach that has been successfully employed to study MMC small-signal stability is the harmonic state-space (HSS) analysis [7], [16]–[19]. Its main advantage, compared to dynamic phasors, is that HSS-based small-signal models can be easily extended to any harmonic order. For instance, in [16] the MMC is seen as a “multi-port” and a simple 2×2 admittance matrix in positive-negative-zero sequence is developed and used to investigate MMC small-signal stability. In [7] the authors developed an HSS model that takes into account the effects of the MMC internal dynamics and control strategies on the impedance at its multi-ports and further validated it by means of experimental measurements. In [17], the authors presented a generalized single-phase MMC model, which eliminates the zero-sequence voltage coupling effect

and is linearized based on HSS theory. In [18], the small-signal stability of voltage-controlled MMCs feeding linear AC systems is considered. By using the HSS modeling method, the AC-side impedance matrices of the MMC with the open-loop and closed-loop voltage control are derived and their relationship is also explicitly given. The authors of [19] focused on the impact of zero-sequence circulating current dynamics on the AC-side dynamics of the MMCs, by developing a complex-valued impedance model for the MMC with three-phase balanced grid voltages. The complex-valued impedance model is based on complex vectors (in contrast with conventional impedance models that are represented by real vectors) and harmonic transfer function matrices.

We present a novel approach to the study of MMC impedance based on the periodic small-signal analysis (PAC) [20]. The term “periodic” refers to the time-varying nature of the small-signal model, which is derived over one period of the large-signal solution of the MMC (in general $1/50\text{ Hz}$ or $1/60\text{ Hz}$). The main advantage of this method, when compared to both dynamic phasors and HSS modeling, is that PAC allows computing the impedance of an MMC without having to explicitly derive a small-signal model of some of its composing parts, such as for example controllers. Often this derivation may be very difficult and performed by pen-and-paper on largely simplified models of the MMC controllers, and by considering an infinite DC bus. These simplifications may require to act on the non-linear differential-algebraic equations of the non-linear MMC model used for time domain stability simulations and to linearise them in a specific working condition. Instead, PAC allows one to numerically obtain a time-varying small-signal model of the MMC that can be used to study the small-signal stability of the system without any intervention on the original time domain simulation model. Additionally, being a numerical method, PAC does not require one to explicitly derive a new small-signal model every time a component of the system under analysis changes because the designer modifies, tailors or substitutes parts of the MMC or the MMC itself is used in different power system configurations (e.g., HVDC or MTDC). This versatility is one of the strongest points of the PAC analysis, which is in sharp contrast with the workflow required, for instance, by the HSS method.

To describe the application of PAC to the study of MMC stability, we build on our previous work [21], in which we used it to develop a dynamic model of a power system incorporating VSC devices: these are described by a non-linear set of switching equations, and the shooting method (SHM) (see [22] and references therein for details on the SHM) is used to compute the behavior of the model at the fundamental frequency of the system (i.e., to determine the previously mentioned *large-signal* periodic solution of the system). The small-signal impedance/admittance model is then computed using the PAC analysis and the vector fitting (VF) algorithm [23], [24] can be employed to derive an analytical formulation of the MMC impedance/admittance model.

The paper is organized as follows. Section II provides a brief description of the MMC model we used, while Section III describes the operating principle of the popular frequency scan technique, and its limitations when it comes to the derivation

of the MMC impedance/admittance matrices. Then, Section IV gives a general introduction to the PAC analysis and derives the generic trans-impedance/admittance matrices computed by PAC (a more detailed description and mathematical derivation of the PAC numerical method is given in Appendix A). To give an idea of the applicability of the method, in Section V we exploit PAC to derive the admittance matrices of two MMCs employed in a HVDC network that connects two AC power systems and study the small-stability of the entire system. Different case studies of increasing complexity are considered to showcase the versatility of the proposed method. Importantly, we show that, in agreement with previous results [16], the derived MMC impedance/admittance model is independent of the grid-side impedance, and captures the interactions between the two AC systems through the HVDC link, which is a quite novel result. Finally, in Section VI we draw some conclusions and discuss possible further applications of our method.

II. MODULAR MULTILEVEL CONVERTER

Figure 1(a) depicts the structure of an MMC made up of three legs, each consisting of an upper and lower arm. Every arm includes a cascading stack of up to several hundreds identical SMS and an RL filter [3]. Regardless of the type of SMS used (e.g., half or full-bridge SM), the gate signals of the IGBTs in each SM originate from a control scheme aimed at fulfilling specific desiderata. This paper adopts the scheme in Fig. 1(c), which comprises four sections. Section ① converts the voltages and currents at the MMC point of common coupling to direct and quadrature components in the positive sequence. A phase-locked loop (PLL) tracks the grid frequency (and, thus, synchronises internal reference signals) by regulating v_q to zero [26]. The outer power loop ② determines the reference DQ axis currents based on specific control objectives, such as active power control [25]. The inner current loop ③ computes the reference voltages at the **a,b,c** terminals necessary for the currents retrieved in ① to track their reference values obtained from ②. Through the inverse Park’s transform, the reference voltages are expressed in the abc-frame [27].

Contrary to traditional VSCs, MMCs also require a scheme to limit circulating currents, which are caused by the inequality among arm voltages. Section ④ replicates the control scheme of [28], which suppresses the double-line frequency negative sequence components of the circulating currents. As a result, this control outputs an additional reference voltage.

Lastly, the reference voltages obtained in sections ③ and ④ are combined with the measured DC-side voltage to obtain the modulation indexes $m_{ua,b,c}$ and $m_{la,b,c}$ of the upper and lower arms of the MMC, respectively. ABC2DQ and DQ2ABC converters are used to manage signals in the MMC controllers (shown in Fig. 1(c)). If a detailed MMC model is adopted, the modulation indexes correspond to specific gate signals, which can be regulated according to a capacitor voltage balancing strategy. In this paper, an average three-phase model of the MMC arms is adopted [29]. In this case, the cascading stack of SMS in each arm of Fig. 1(a) is represented through a lumped capacitor C_m and a voltage-dependent voltage source, as shown in Fig. 1(b).

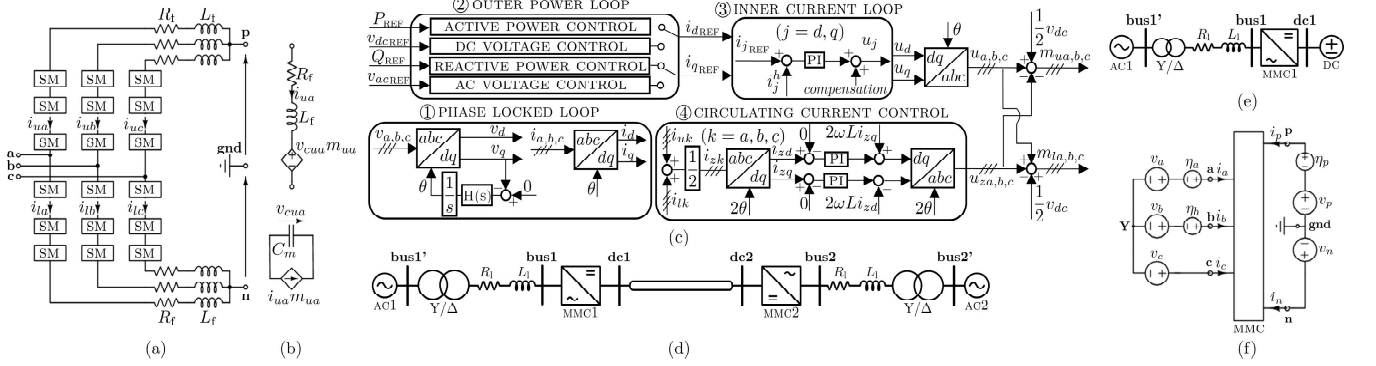


Fig. 1. (a) High-level block schematic of the MMC model. (b) Generic arm representation in the MMC average model for phase a, upper arm. (c) MMC control scheme. (d) - (e) Detailed and simplified schematics of the DCS1 HVDC test system described in [25]. (f) MMC representation as a 5-terminal component.

III. FREQUENCY SCAN

The simulation technique known as *frequency scan* [9], and implemented in several power system simulators used in the industry (e.g., EMTP-RV and POWERFACTORY [30]), is based on a three-step numerical algorithm. The power flow solution of the power system model is computed in the first step, and its dynamic elements (i.e., those described by differential algebraic equations (DAEs), such as for example synchronous generators) are initialised in the second step. By doing so, an *equilibrium point* of the power system model is identified. The power system model is then *linearised* around this very equilibrium point, and its small-signal solution is computed by sweeping (*scanning*) a system parameter (i.e., *frequency*). Frequency scan thus requires that the power system model admit a steady-state solution which is an equilibrium point and therefore the latter must be formulated so that, if a steady-state solution exists, it must be an equilibrium point.

In principle, a power system described in the abc-frame does not admit an equilibrium point as a steady-state solution but a *periodic orbit*. It is well known that, if one applies the Park's transform [27] to the abc-model, an equivalent model is obtained in the dq0-frame. If the original periodic solution in the abc-frame (i) is not characterised by harmonics and (ii) exhibits the positive sequence only, the periodic orbit solution in the abc-frame transforms into an *equilibrium point* in the dq0-frame. Frequency scan is thus successfully applied to the power system model in the dq0-frame. In all other cases, we have a periodic orbit in the abc-frame, transformed into another periodic orbit in the dq0-frame, and frequency scan can not be applied.

The MMC model described in Section II and shown in Fig. 1 is mostly formulated in the abc-frame but some of its sub-systems (mainly controllers, as it happens in a real design) are formulated in the dq0-frame. The resulting model is non-linear and also potentially affected by the negative sequence (consider for instance the presence of possible unbalances in the AC grid). Therefore, since the model is formulated in a mixture of the abc- and dq0-frames, a periodic steady-state solution is obtained. This implies that the frequency scan technique cannot be used to compute the equivalent MMC impedance/admittance matrix. To force its usage, the

model must be deeply simplified in order to obtain a solution represented by a simple equilibrium point in the dq0-frame. This is what is done in several papers (see for example [31]) but requires a significant amount of effort that can be avoided by applying our proposed method. As anticipated in the Introduction, a good numerical tool able to compute the impedances of the MMC model without resorting to any simplification is the PAC method, which we present in the next section. As shown in the following, the PAC can take into account intermodulation and up- and down-conversion of a perturbing signal in the frequency spectrum. For example, it can compute how a low frequency (e.g., 1 Hz) perturbation in the HVDC link can be up-converted to 50 + 1 Hz in the AC system.

IV. PERIODIC SMALL-SIGNAL ANALYSIS

The dynamical evolution of a generic electr(on)ic circuit or system in the time domain can be typically modeled by a set of non-linear DAEs [32], [33]. In principle, if these DAEs are of index-1 [34], a state-space form with a minimal set of variables leading to a system of ordinary differential equations (ODEs) can be identified. In general, it cannot be done in explicit form, for instance if the algebraic constraints are highly non-linear, but this formulation exists theoretically, and when the explicit form exists, it can be profitably used to reduce complexity in deriving results.

This paper focuses on circuits that operate at periodic steady-state and are described by non-linear and time-varying index-1 DAEs: MMCs belong to this class of circuits. The goal is to analyze the effect of periodic small-signal perturbations applied to these periodically working circuits and to derive transfer functions that help designers in the circuit design phase. To do so, we resort to periodic small-signal analysis (PAC). It is an extension of the standard small-signal analysis, which is used to calculate the small-signal response of a circuit in the neighborhood of an equilibrium point [20].

Consider the following index-1 DAE describing the dynamics of a periodically forced circuit (with period $T = 1/f_o = 2\pi/\omega_o$)

$$\frac{d}{dt} q(t, y) + j(t, y) = \emptyset , \quad (1)$$

where $\emptyset \in \mathbb{R}^N$ with N the number of equations (differential and algebraic). It reduces to an ODE if all the entries of the $q(t, y)$ vector are non-null. If the circuit steady-state is periodic, an orbit $y_s(t) = y_s(t + T) \in \mathbb{R}^N$ (*large-signal solution*) exists that solves (1). In our case, $y_s(t)$ represents the periodic solution of the MMC at both the AC and DC sides, when it works in a steady-state condition. A small additive perturbation $\eta(t) \in \mathbb{R}^M$, which is obtained by combining the effects of M small-signal inputs, is assumed to act as

$$\frac{d}{dt}q(t, y) + j(t, y) = \Lambda\eta(t), \quad (2)$$

where $\Lambda \in \mathbb{R}^{N \times M}$ is a constant matrix. We are interested in estimating how $\eta(t)$ affects $y(t)$. With this aim, assume that the effects of $\eta(t)$ translate into writing the solution of the original non-linear circuit as $y(t) = y_s(t) + y_\eta(t)$. In other words, we assume that the effects of the small-signal perturbation *superimpose* to the large-signal (unperturbed) solution. In the light of the above, system (1) is linearized along $y_s(t)$ (i.e., along a periodic working cycle of the circuit), thereby obtaining

$$\frac{d}{dt} \left[\underbrace{\frac{\partial q(t, y)}{\partial y} \Big|_{y=y_s}}_{C(t)} y_\eta \right] + \underbrace{\frac{\partial j(t, y)}{\partial y} \Big|_{y=y_s}}_{G(t)} y_\eta = \Lambda\eta(t), \quad (3)$$

where $y_\eta(t)$ is the *small-signal solution* and matrices $C(t)$ and $G(t)$ are characterized by T -periodic entries.

The literature describes several techniques to obtain the periodic steady-state solution of (1) [35] and the (small-signal) solution of (3). In this paper, we resort to the shooting method (SHM), which is formulated in the time-domain [36]¹. For space reasons, we do not recall SHM (which was recently used also in [33]) but we provide in Appendix A some specific hints about the small-signal time-domain solution, which is a key aspect of PAC.

Assume that the small-signal input to system (3) is $\eta(t) = \Xi \sin(2\pi t/T_\eta + \psi)$, where Ξ is an M real-element vector, and $T_\eta \in [T_\eta^{\min}, T_\eta^{\max}]$, where these interval extremes define the bandwidth of the small-signal we are interested in. We vary

¹In general, this is the only available method whenever the circuit is switching or described by an Analog Mixed Signal (AMS) model. In these cases, it is necessary to resort to an extension toward hybrid dynamic systems of SHM [37], [38].

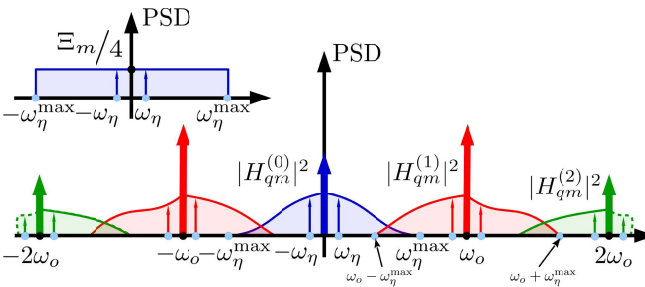


Fig. 2. Sketch of both the PSD of the m -th component of $\eta(t)$ (upper-left inset) and of $|H_{qm}^{(k)}|^2$ transfer functions from the m -th component of $\eta(t)$ to the q -th component of $y_\eta(t)$ centered at $\pm 2\pi kf_0$. $\omega_\eta = 2\pi/T_\eta$.

T_η in the selected interval, thus achieving a set of small-signal solutions $y_\eta(t; T_\eta)$. Since (3) is a set of linear time-varying periodic DAEs, the spectrum of $y_\eta(t; T_\eta)$ contains frequencies of the form $2\pi kf_0 \pm 2\pi/T_\eta$, i.e., *frequency is folded* at kf_0 harmonics of the periodic large-signal solution [39]. This is exemplified in Fig. 2, where the harmonics at $2\pi kf_0$ refer to the large-signal solution. By performing the Fourier transform of $y_\eta(t; T_\eta)$, it is possible to derive the modulus and the phase of each $H_{qm}^{(k)}(\omega)$ transfer function for $q = 1, \dots, N$ and $m = 1, \dots, M$ (see Fig. 2). $H_{qm}^{(k)}(\omega)$ represents the transfer function from the m -th component of $\eta(t)$ to the q -th component of $y_\eta(t)$ centered at $\pm 2\pi kf_0$. In general, the effects of these contributions should be combined at all those frequency values at which overlaps are observed. This is exemplified in Fig. 2 by the superposition of $H_{qm}^{(0)}(\omega)$ with $H_{qm}^{(1)}(\omega)$, and of $H_{qm}^{(1)}(\omega)$ with $H_{qm}^{(2)}(\omega)$. In formula it reads

$$\hat{y}_\eta(\omega) = \sum_k \underbrace{\begin{bmatrix} H_{11}^{(k)}(\omega) & \dots & H_{1M}^{(k)}(\omega) \\ \vdots & \ddots & \vdots \\ H_{N1}^{(k)}(\omega) & & H_{NM}^{(k)}(\omega) \end{bmatrix}}_{H^{(k)}(\omega)} \hat{\eta}(\omega), \quad (4)$$

where $\hat{y}_\eta(\omega)$ (resp. $\hat{\eta}(\omega)$) is the Fourier transform of $y_\eta(t)$ (resp. $\eta(t)$)². If one is interested in analysing what happens around the generic $2\pi kf_0$ harmonic, the $H^{(k)}(\omega)$ contributions with $k \neq p$ can be ignored if they are negligible w.r.t. $H^{(p)}(\omega)$. This implicitly reflects on the summation index in (4).

V. NUMERICAL RESULTS

In this section we fully exploit PAC: to this end, we adopt both a simplified and a detailed version of a point-to-point HVDC system. Figure 1(d) depicts the detailed test system, whose specifications can be found in [25]. It comprises two AC grids, one HVDC link, and two MMCs. The MMC2 works in the DC-SLACK mode to keep the DC link voltage constant at ± 200 kV, while the MMC1 works in PQ mode and nominally injects 400 MW in the DC grid. Reactive power exchange is zero for both MMCs. On the contrary, in the simplified version of the test system shown in Fig. 1(e), an infinite DC bus (which keeps the DC link voltage fixed at ± 200 kV) replaces what is originally connected to the right of bus **dc1**.

We want to stress that our goal here is not to investigate the HVDC system in use (and, for instance, improve its operation by implementing more advanced controls), but rather to show the features of PAC by applying it to the previously described test systems. In the following, we comment on the characteristics of the specific transfer functions and possible interesting electrical aspects enlightened by PAC.

The results presented in this Section were obtained by resorting to our circuit and system simulator PAN [40], [41]³.

²It is worth mentioning that, if one is interested in the transfer functions relating a subset of the elements of $\eta(t)$ to a subset of the elements of $y_\eta(t)$ (or a linear combination of them) it is sufficient to properly select and combine a subset of the elements of each $H^{(k)}(\omega)$ matrix.

³The files necessary to simulate the HVDC system with PAN simulator are available on GitHub at the address <https://github.com/danielelinaro/mmc-pac.git>.

A. The first basic example

To introduce the operating principles of PAC on a complex system, we start with the configuration shown in Fig. 1(f), where the block labeled as MMC is composed of the (a), (b), and (c) blocks in the same figure. Its external connections are those of the (a) block. Neglect momentarily the η_a , η_b , and η_p small-signal voltage sources. By referring to the circuit in Fig. 1(f), we can write $i_a + i_b + i_c = 0$ and $i_p + i_n = 0$. By regarding the MMC as a peculiar 5-terminal element, this implies that (i) only three currents are necessary to describe its behavior, and (ii) three voltages must be chosen to drive it (two among v_a , v_b , and v_c at the AC side, one between v_p and v_n at the DC side). In this paper, we choose the (v_a, v_b, v_p) and (i_a, i_b, i_p) voltages and currents. Our goal is to study the effects of the η_a , η_b , and η_p small-signal voltage sources in Fig. 1(f) on the periodic behavior of the circuit. Through PAC, a matrix of transfer functions can be obtained in the form

$$\begin{bmatrix} \hat{i}_{a_n} \\ \hat{i}_{b_n} \\ \hat{i}_{p_n} \end{bmatrix} = \underbrace{\begin{bmatrix} Y_{aa}^{(0)} & Y_{ab}^{(0)} & Y_{ap}^{(0)} \\ Y_{ba}^{(0)} & Y_{bb}^{(0)} & Y_{bp}^{(0)} \\ Y_{pa}^{(0)} & Y_{pb}^{(0)} & Y_{pp}^{(0)} \end{bmatrix}}_{Y^{(0)}} \begin{bmatrix} \hat{\eta}_a \\ \hat{\eta}_b \\ \hat{\eta}_p \end{bmatrix}, \quad (5)$$

where Y is used instead of H (see (4)) since the entries are admittances (from hereon, for the sake of brevity, the frequency-dependency of each entry of the matrix is omitted). This represents the small-signal model of the MMC in this specific configuration and PAC provides the entries of this matrix in numerical form. One may then use VF to obtain an approximate formulation in closed-form, as described in Section V-D⁴.

Consider now the simple power system shown in Fig. 1(e), in which we first applied PAC. Compared to Fig. 1(f), in this case the v_a , v_b , v_c , η_a and η_b voltage sources are located in the three phases of the generator in the AC1 grid. These sources have impedances connected in series. On the contrary, the v_p , v_n , and η_p sources are in the DC infinite bus. Due to space reasons, hereafter we only show the results pertaining to some of the entries of $Y^{(0)}$ matrix in (5). In this case, the selected transfer functions are shown by the black traces in Fig. 3. Some peaks in the magnitudes of the transfer functions are visible at about 23 Hz, 61 Hz, and 152 Hz; due to its magnitude the last one could give rise to some resonance problems.

We then added an HVDC link between bus **dc1** and the infinite DC bus in Fig. 1(e)⁵. The cables of the HVDC link, whose parameters are reported in [25], were modeled with the

⁴Since $i_a + i_b + i_c = 0$, the zero-component of the currents in Fig. 1(e) is zero. This is not the case if the Y node is connected to ground. If so, another small-signal voltage source must be added, and the size of the matrix in (5) increases to 4×4 . Despite this, the application of the PAC remains straightforward. We mention this since [17], [19] derived impedance models of a three-phase, four-wire MMC, where its DC and AC sides were grounded to provide a circulation path for the zero-sequence current. This path does not exist in reality, as MMCs are three-phase, three-wire systems. Thus, to force the zero-sequence current on the MMC AC side to zero in order to carry out the analysis, [17] introduced a fictitious zero-sequence voltage compensation. On the contrary, PAC requires no additions of this sort.

⁵Considering the power system in Fig. 1(d), the same circuit is obtained by replacing what is connected to the right of bus **dc2** with an infinite DC bus.

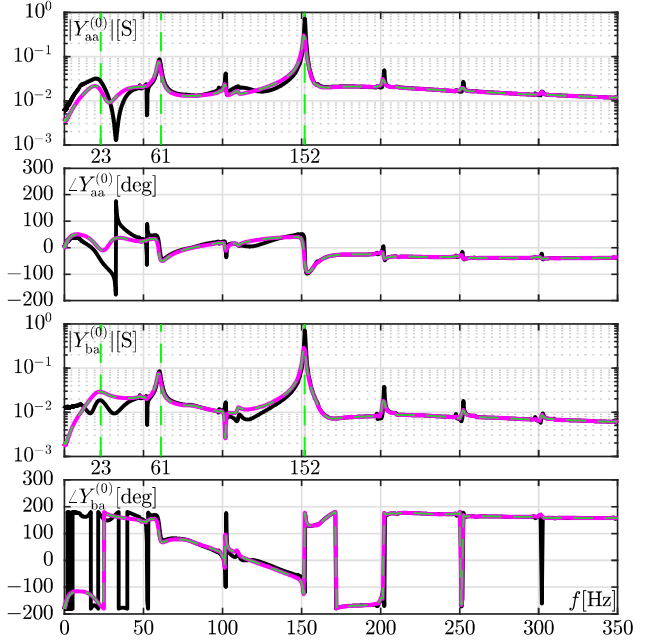


Fig. 3. The magnitude and phase of the $Y_{qm}^{(0)}$ admittance entries of the $Y^{(0)}$ matrix in Eq. (5). The set plotted with solid black lines refers to the power system configuration shown in Fig. 1(e). The set plotted with solid magenta lines refers to the power system configuration in Fig. 1(e) with an infinite DC bus replacing what is connected on the right of the DC2 bus in Fig. 1(d). The set plotted with dashed green lines refer to the DCS1 system shown in Fig. 1(d). By counting panel from top: panel 1: magnitude of $Y_{aa}^{(0)}$; panel 2: phase of $Y_{aa}^{(0)}$; panel 3: magnitude of $Y_{ba}^{(0)}$; panel 4: phase of $Y_{ba}^{(0)}$.

detailed state-space equivalent model described in [42]. We repeated the PAC analysis and computed the same admittances of the first example. The results, shown by the magenta traces in Fig. 3, are superimposed to those of the previous case. The differences between the black and magenta traces reveal that the admittance at the AC side of MMC1 cannot be accurately computed by representing its DC side only with an infinite DC bus instead of a proper HVDC system (i.e., HVDC link and possibly also MMC2). This is what was done for example in [16], [43] (i.e., the DC side was neglected), and here we have verified that this is not admissible in our case.

B. The complete DCS1 test system

We now consider the full DCS1 system depicted in Fig. 1(d), composed of two MMCs and an HVDC link. As in the previous cases, we injected a small-signal tone through η_a in the AC1 grid and performed a PAC analysis. The $Y_{aa}^{(0)}$ and $Y_{ba}^{(0)}$ admittances of MMC1 obtained in this case are given by the green traces in Fig. 3. The magenta and green traces almost perfectly overlap, which suggests that the adoption of the real MMC2 - or, in its stead, of an infinite DC bus in series with an HVDC link - leads to almost identical results in terms of $Y_{aa}^{(0)}$ and $Y_{ba}^{(0)}$.

The latter case, however, does not allow analyzing interactions between AC1 and AC2 grids. Besides, perturbations in the AC1 system close to the synchronous frequency, may be down-converted in frequency by MMC1, propagate through

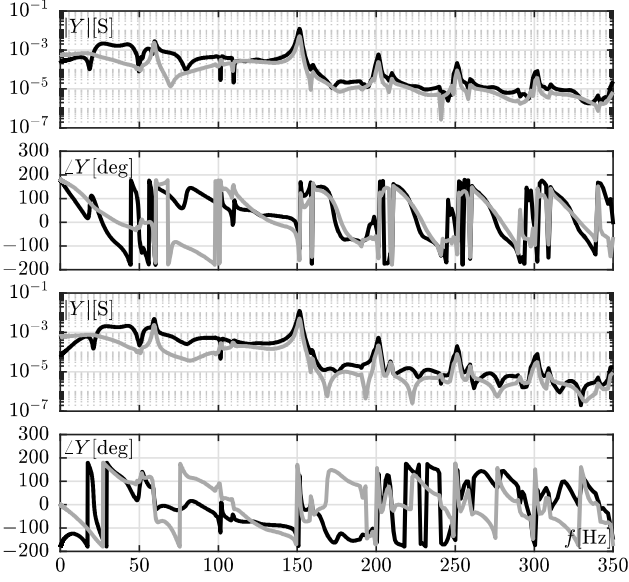


Fig. 4. Panel are listed from top. Panel 1: moduli of $Y_{a^{\text{slk}},a^{\text{pq}}}^{(0)}$ (black) and $Y_{b^{\text{slk}},a^{\text{pq}}}^{(0)}$ (gray). Panel 2: phases of $Y_{a^{\text{slk}},a^{\text{pq}}}^{(0)}$ (black) and $Y_{b^{\text{slk}},a^{\text{pq}}}^{(0)}$ (gray). Panel 3: moduli of $Y_{a^{\text{pq}},a^{\text{slk}}}^{(0)}$ (black) and $Y_{b^{\text{pq}},a^{\text{slk}}}^{(0)}$ (gray). Panel 4: phases of $Y_{a^{\text{pq}},a^{\text{slk}}}^{(0)}$ (black) and $Y_{b^{\text{pq}},a^{\text{slk}}}^{(0)}$ (gray).

the HVDC link, be up-converted by MMC2, and interact with the AC2 system. The same may occur the other way round, possibly with different magnitudes and/or phases due to the different control functions implemented in the two MMCs. To verify the above statement, we injected a small-signal tone in phases a and b, first of the AC1 and later of the AC2 systems, and computed the corresponding cross admittances. We use the $^{\text{pq}}$ and $^{\text{slk}}$ symbols to refer to transfer functions of the AC1 and the AC2 systems, respectively. The obtained $Y_{a^{\text{slk}},a^{\text{pq}}}^{(0)}$, $Y_{b^{\text{slk}},a^{\text{pq}}}^{(0)}$ and $Y_{a^{\text{pq}},a^{\text{slk}}}^{(0)}$, $Y_{b^{\text{pq}},a^{\text{slk}}}^{(0)}$ admittances are shown in Fig. 4. By observing these traces, we see that there is some (small) coupling between the AC1 and AC2 systems, since magnitudes are not null. Couplings are similar as indicated by comparable magnitude values. Note that these results cannot be obtained with a frequency scan, since it does not cope with up- and down-conversion of the injected small signal.

C. The HVDC link

We now consider the DC side of MMC1 in three different cases (a, b, and c). In case (a), described in Sec. V-A, we connect the DC side of MMC1 to an infinite DC bus. In case (b), described in the same subsection, we consider an HVDC cable in series with an infinite DC bus. Both in case (a) and (b) the small-signal tone is injected by the η_p source inside the infinite DC bus. Lastly, in case (c) we study the DCS1 (full system) described in Sec. V-B and insert the η_p small-signal generator between the P node of MMC1 (see the block in Fig. 1(f)) and the HVDC cable.

In Fig. 5 we report the real and imaginary parts of the $Y_{pp}^{(0)}$ admittances of the three cases. At low frequencies, the admittance is of resistive/capacitive type (i.e., negative

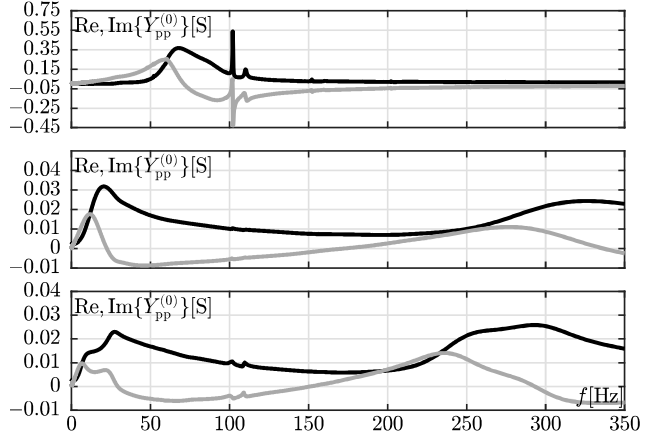


Fig. 5. The real (black) and imaginary (gray) components of the $Y_{pp}^{(0)}$ admittances of the (a), (b) and (c) case studies. Real and imaginary parts of $Y_{pp}^{(0)}$ are displayed in panels from top for the (a), (b) and (c) cases.

imaginary part) in all cases. It is also worth pointing out that the real part of three admittances is never negative, which is a general indication of the fact that MMC1 is not prone to DC side instabilities. This aspect was considered in recent works [44]–[46], which highlighted the importance of accurate cable modeling when studying DC side stability [42]. The frequency-dependence of the resistance and inductance due to skin effect improves stability margins: although the capacitive part of the admittance of the MMC may fall in some frequency ranges due to resonance phenomena, the cable resistance is sufficiently high and the inductance is sufficiently low to prevent the negative resistance of the MMC from manifesting.

D. Stability analysis through vector fitting

Once the admittances of the MMC have been derived numerically, they can be represented in closed-form with the VF algorithm, which then allows performing several stability analyses. To showcase this feature, we considered once again the DCS1 system and investigated as an example the possible instability triggered by the insertion of inductor-based Fault Current Limiters (FCLs) at each pole of the DC side of MMC1. This issue has been recently reported for instance in [31], [45], [46], where the authors showed that a too large inductance leads to instabilities [45], [46]. In [31] the authors came to the opposite conclusion (i.e., a too small inductance value leads to instabilities). It thus seems that an interval of inductance values exists in which the insertion of a reactor limits the DC short circuit current, and does not trigger instability phenomena.

The important aspect is that the analysis that we propose here is performed after having derived an analytical model of the two MMCs connected through an HVDC link. Such analytical model is obtained by applying VF to the numerical results provided by PAC analysis of the complex model shown in Fig. 1(d). In principle, if this analytical model is sufficiently simple, it allows the designer to perform a conventional pen-and-paper analysis or with a programming language such as MATLAB or Python. In our case, we used simple MATLAB scripts and toolbox functions to perform a parametric stability

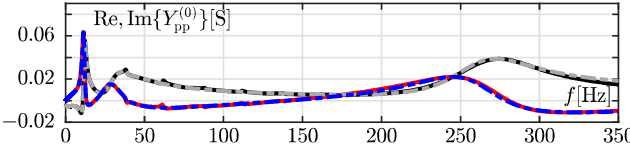


Fig. 6. The real and imaginary parts of $Y_{pp}^{(0)}$ of the modified DCS1 test system. Black and red traces refer respectively to the real and imaginary part of Y_{pp}^0 obtained numerically with PAC, while the gray and blue lines correspond to the results obtained with VF.

analysis where we varied the value of the reactor connected in series to the poles of the HVDC link mentioned before in the interval of values used in practice. To this end, we computed again the $Y_{pp}^{(0)}$ admittance in the (c) case of the previous section by resorting to PAC and a modified version of the DCS1 system. In this version, we varied the power setpoint of MMC1 with 6 s-long steps of -100 MW (reaching -800 MW) and reduced the integral gain of the PI controller I_{K_I} of the MMC inner current loop from 149 to 30 (Table 6.10 of [25] shows the original control parameters)⁶.

Figure 6 depicts the real and imaginary parts of $Y_{pp}^{(0)}$, obtained with PAC and VF, when the MMC reference power reaches -800 MW. We see that there is a negative peak of the real part of $Y_{pp}^{(0)}$ at about 11 Hz⁷. The VF process required 10 poles for the closed-form results to match the numerical ones by PAC. VF thus gave us the analytic expression of $Y_{pp}^{(0)}$ that we used in (6).

If an inductor is connected at each pole of the DC side of MMC1, the equivalent DC side admittance $Y_{pp,new}^{(0)}$ becomes:

$$Y_{pp,new}^{(0)} = \frac{Y_{pp}^0 \frac{1}{i\omega L_{dc}}}{Y_{pp}^0 + \frac{1}{i\omega L_{dc}}} = \frac{Y_{pp}^0}{1 + i\omega L_{dc} Y_{pp}^0}, \quad (6)$$

where L_{dc} is the inductance of the fault current limiter. The expression in (6) is equivalent to the closed-loop transfer function of a feedback system, where Y_{pp}^0 and $i\omega L_{dc}$ lie respectively in the forward and feedback paths. The root locus of the system allows studying how the poles vary with respect to L_{dc} . We expect that, as L_{dc} increases, some poles move to the right half of the s-plane, making the system unstable.

The top panels of Fig. 7 show the root locus of the system in Eq. (6). In the top right panel, the *, \square , \diamond , and \triangle markers indicate how some poles vary when L_{dc} is respectively equal to 50, 75, 100, and 125 mH. These markers show that the system is surely unstable for $L_{dc} \geq 100$ mH (i.e., some poles lie in the right half of the s-plane). For instance, the bottom

⁶This amendment, albeit debatable from a design standpoint, was implemented to reduce stability margins and observe an instability caused by the insertion of inductor-based FCLs of plausible inductance.

⁷The results in Figure 6 are consistent with what was reported in [45], [46]. We performed also a PAC analysis in a wider range of frequencies that extended up to 10 kHz. This result is not reported in the paper. What we found is that there is not any negative impedance effect at high frequencies (some kHz) as described in [31], at least for our design. From our standpoint this is an expected result, since the signals driving the MMC are low-pass filtered (these filters are not shown in Fig. 1) and the cut-off frequencies are well below those at which negative impedance manifests in [31]. Note that due to low-pass filtering, the two MMCs are no longer able to maintain their functionalities, i.e., to act as DC-SLACK and PQ, at frequencies well above these cut-off ones.

panels of Fig. 7 depict the Nyquist diagram of the open-loop transfer function in (6) for $L_{dc} = 100$ mH. The point $(-1,0)$ is encircled, confirming system instability⁸.

To add a final proof of instability, we performed time-domain simulations of the test system by considering the previously mentioned values of inductance L_{dc} . Based on the root loci in Fig. 7, we expect that when L_{dc} is equal to 50 or 75 mH the system is still stable when active power exchange amounts to -800 MW. On the contrary, when L_{dc} is equal to 100 or 125 mH, instability occurs. This is confirmed by the results shown in Fig. 8. For instance, when $L_{dc} = 100$ mH, the system becomes unstable when the reference power reaches -800 MW (i.e., the DC-side voltage diverges). On the contrary, when $L_{dc} = 125$ mH, instability occurs starting from a power reference of -700 MW. In the unstable cases, the divergence in the DC-side voltage is evident. On the contrary, the power exchange is bounded between two extremes (see the lower panel for $t \geq 42$ s, for instance): this is because of the presence of limiters in the PI controllers inside the MMC scheme.

E. From baseband to the second harmonic

To show the potentiality peculiar to PAC, we consider once again the test system in Fig. 1(e). In particular, we analyse the effects of the frequency up-conversion (folding) of the small-signal η_a at $2f_0$ (i.e., in the right-side band of the second harmonic) on the small-signal current flowing through η_p in the infinite DC bus. We know that, due to the periodic working mode of the MMC and circulating currents, a second harmonic component may be present in the DC line current. The obtained $Y_{pa}^{(2)}$ is shown in Fig. 9. We underline that frequencies on the x-axis must be read as $2f_0 + 1/T_n = 100$ Hz + $1/T_n$. For example, a small-signal perturbation at $1/T_n = 1$ Hz of the η_a source in the AC1 grid thus folds at 100 Hz + 1 Hz in the frequency axis.

⁸For the sake of completeness, we performed PAC and VF for each power reference step shown in Fig. 8. We then drew the corresponding Nyquist plots (not reported here for space reasons) by letting $L_{dc} = 100$ mH. This was done to verify that the point $(-1,0)$ in the Nyquist plot is encircled (i.e., instability occurs) only when the reference power reaches -800 MW.

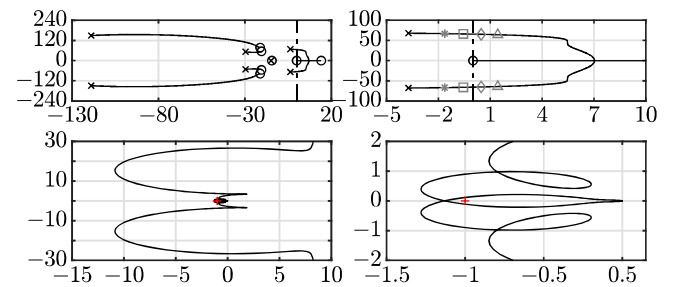


Fig. 7. Upper panels: root locus of (6) as a function of L_{dc} (left) and its inset (right) (stable poles that lie further away in the left half plane are not shown). In the inset, the *, \square , \diamond , and \triangle markers indicate the value of some poles in the root locus when L_{dc} is respectively equal to 50, 75, 100, and 125 mH. Lower panels: Nyquist diagram of $i\omega L_{dc} Y_{pp}^0$ when $L_{dc} = 100$ mH (left) and its inset (right). The + marker denotes the point $(-1,0)$. x-axis: real part; y-axis: imaginary part.

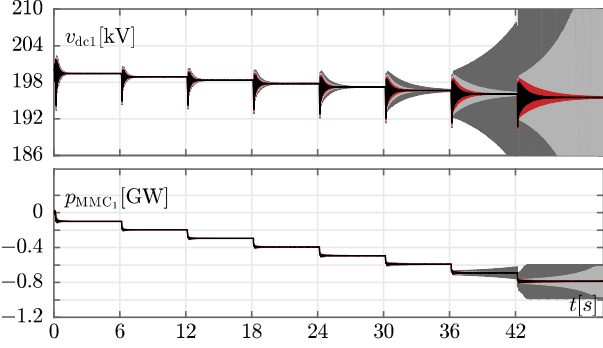


Fig. 8. Simulation results of the modified DCS1 system obtained by inserting an inductance L_{dc} at each pole of the DC side of MMC1. Upper panel: MMC1 positive pole to ground voltage. Lower panel: MMC1 active power exchange. In the first 150 ms of simulation the entire system undergoes a turn-on phase. In both panels, the black, red, grey and dark grey lines correspond to simulations with a value of L_{dc} respectively equal to 50, 75, 100, and 125 mH.

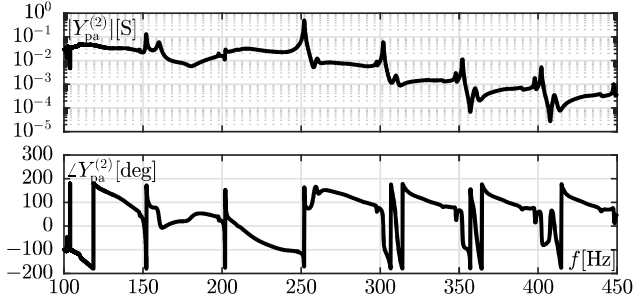


Fig. 9. The module and phase of the $Y_{pa}^{(2)}$ admittance of the power system configuration shown in Fig. 1(e). Upper panel: module of $Y_{pa}^{(2)}$. Lower panel: phase of $Y_{pa}^{(2)}$. The superscript ⁽²⁾ indicates frequency up-conversion at the second harmonic.

F. Unbalanced AC grid

As already stated, versatility is one of the strongest points of the PAC analysis. For instance, if the effect of new controls and/or system parameters needs to be examined, simulations can simply be rerun to derive new impedance/admittance MMC matrices through the adoption of PAC, without the need to perform extensive pen-and-paper calculations. The same holds true in the case of unbalanced operating conditions. To validate this last statement, we modified system AC1 in Fig. 1(e). In general, the AC grids in this paper are modeled based on [25] as three-phase balanced voltage sources in series with an impedance. In this specific case, however, the voltage associated with phase a was slightly changed as shown by the black line in the top panel of Fig. 10 to generate unbalanced operating conditions. The resulting phase currents when MMC1 injects 400 MW in the DC grid are shown in the bottom panel of the same figure.

Figure 11 compares for example the $Y_{pa}^{(0)}$ admittance obtained during both balanced and unbalanced operating conditions. The almost identical traces indicate that the perturbation on phase a acts on the HVDC point-to-point link current ripple in the same way, i.e., the large signal voltage unbalance acts on the HVDC link current in an almost linear way: for

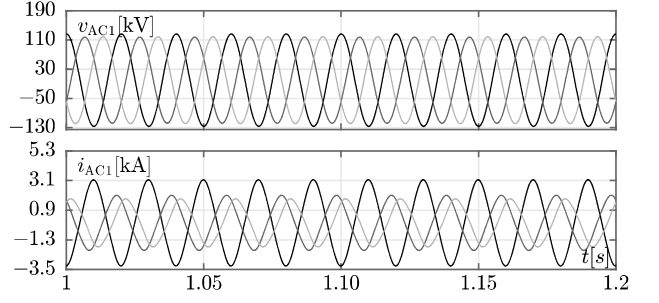


Fig. 10. Phase voltages (upper panel) and currents (lower panel) of the AC1 system in Fig. 1(e) under unbalanced operating conditions. In both panels, the black, dark gray, and light gray lines refer respectively to phases a, b and c.

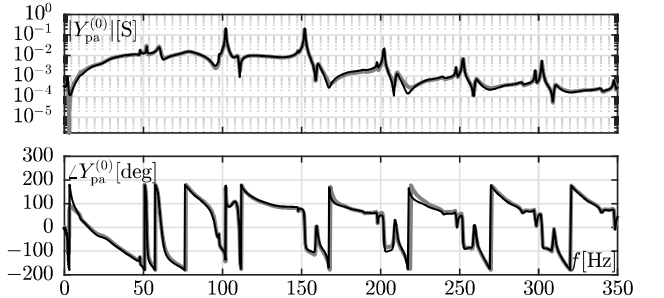


Fig. 11. The module and phase of the $Y_{pa}^{(0)}$ admittance of the power system configuration shown in Fig. 1(e) under balanced (black solid line) and unbalanced (gray dashed line) operating conditions. Upper panel: module of $Y_{pa}^{(0)}$. Lower panel: phase of $Y_{pa}^{(0)}$.

example doubling the magnitude of the unbalancing voltage leads to a doubling of the current ripple of the HVDC link.

VI. CONCLUSION

This paper has presented the periodic small-signal analysis (PAC) tool to derive the transfer functions between nodes and ports both on the AC or DC side of modular multilevel converters (MMCs), connected, for instance, by an HVDC point-to-point link. We have computed several transfer functions and among these the admittance of the DC side of the PQ MMC in the HVDC link. We have shown that in some frequency intervals the MMC can have negative impedance and be prone to instability. We have shown how the insertion of an inductor-based FCL can trigger instability by performing a parametric pole analysis. To efficiently do this, the numerical transfer function computed by PAC was fitted by using the VF technique. The obtained algebraic equivalent expression was used in MATLAB to perform both the Nyquist stability analysis and the root-locus analysis. The obtained results were validated by means of accurate transient stability studies. In all these analyses, we used detailed three-phase models of MMCs including outer power loop and inner current loop controllers, circulating current suppression strategies, and PLLs.

APPENDIX A PERIODIC SMALL-SIGNAL ANALYSIS IN BRIEF

Without loss of generality, assuming that (1) reduces to a set of ODEs, as a by-product of SHM itself, a finite set of

samples of the $\Phi(t, t_0)$ state transition matrix [47] of the circuit, computed along its periodic solution, is available. These samples are known at possibly not equispaced time instants t_h ($h = 0, \dots, H$) being $t_H = T$. To evaluate $y_\eta(t)$ for $t \in [t_0, t_0 + T_\eta]$ one can write

$$y_\eta(t) = \Phi(t, t_0) \int_{t_0}^t \Phi^{-1}(\tau, t_0) \Lambda \eta(\tau) d\tau , \quad (7)$$

where $\eta(t) = \eta(t + T_\eta) = \eta(t + \nu T)^9$. Assuming that the monodromy matrix $\Psi = \Phi(t_0 + T, t_0)$ can be diagonalized as $V \Delta V^{-1}$ (this is generally the case dealing with well posed circuits), by resorting to the Floquet-Lyapunov factorization [48], one can write

$$\begin{aligned} F &= \frac{1}{T} V \log(\Delta) V^{-1} \\ L_F(t, t_0) &= \Phi(t, t_0) V \Delta - \frac{t - t_0}{T} V^{-1} , \end{aligned} \quad (8)$$

where F is one of the infinitely many solutions of the equation $e^{FT} = \Psi$, $L_F(t + T, t_0 + T) = L_F(t, t_0)$, and $L_F(T + t_0, t_0) = L_F(t_0, t_0) = \mathbb{1}_N$ (being $\mathbb{1}_N$ the $N \times N$ identity matrix). The entries of $L_F(t, t_0)$ are thus known at $t_{hn} = t_h + nT$, for $h = 0, \dots, H$ and $n = 0, \dots, \nu - 1$. Equation (7) can be rewritten as

$$y_\eta(t) = L_F(t, t_0) V \int_{t_0}^t \Delta \frac{t - \tau}{T} (L_F(\tau, t_0) V)^{-1} \Lambda \eta(\tau) d\tau . \quad (9)$$

The $(L_F(\tau, t_0) V)^{-1}$ matrix can be expressed through the Fourier decomposition of each one of its entries as

$$(L_F(\tau, t_0) V)^{-1} = \sum_{r=0}^{\infty} C_r \underbrace{\text{diag} \left(e^{\frac{2\pi r i t}{T}} \dots e^{\frac{2\pi r i t}{T}} \right)}_{E_r(t)} , \quad (10)$$

where C_r is an $N \times N$ complex elements matrix, and $E_r(t)$ are $N \times N$ elements diagonal matrices. As a consequence, (9) can be finally transformed into

$$y_\eta(t) = L_F(t, t_0) V \sum_{r=0}^{\infty} C_r B_r(t) , \quad (11)$$

where $B_r(t)$ are diagonal matrices whose (k, k) -element ($k = 1, \dots, N$) is

$$(B_r(t))_{k,k} = \int_{t_0}^t \Delta_{k,k} - \frac{t - \tau}{T} e^{\frac{2\pi r i t}{T}} (\Lambda \eta(\tau))_k d\tau . \quad (12)$$

In practice, the summations in Eqs. (10) and (11) are truncated to R terms and the integral in (12) may be solved in closed-form [49].

⁹ In the following, we assume $\nu \in \mathbb{Z}$ since it is more practical, but the proposed approach can be easily generalized for $\nu = \frac{\nu_N}{\nu_D} \in \mathbb{Q}$. In that case, $y_\eta(t)$ is computed in the time interval $[t_0, t_0 + \nu_D T_\eta] \equiv [t_0, t_0 + \nu_N T]$.

APPENDIX B VECTOR FITTING

The vector fitting (VF) method allows describing a measured or calculated frequency domain response $f(s)$ through a rational transfer function. This algorithm was originally adopted to build frequency-dependent models of cables and transformers [24]. Since then, a wide array of applications has made use of this method. For example, the authors in [50] use VF and measured data to derive a black-box model of a dynamic load. In [51], the VF method automatically identifies the electrical components of a circuit. The algorithm was also applied in [42] to derive a frequency-dependent lumped parameter model of cables necessary for accurate state-space modeling of HVDC systems. VF was also recently used to model the transfer function of a grid-following inverter [52].

In a nutshell, VF approximates $f(s)$ through the partial fraction expansion

$$f(s) = \sum_{n=1}^N \frac{c_n}{s - a_n} + d + sh , \quad (13)$$

where N is the order of approximation, while a_n and c_n are respectively the poles and residues of the transfer function. The terms d and h , corresponding to a constant gain and a frequency-proportional term, are optional, as their presence depends on the fitted frequency response. VF estimates the parameters above by initially guessing the approximation order N and sequentially solving two stages.

The first stage derives the poles a_n by adopting an iterative procedure that relies on their initial estimate (typically logarithmically spaced over the frequency range of interest) and a scaling function. In each iteration, poles are relocated until a convergence criterion is attained. Should this criterion not be satisfied after a given number of iterations, the algorithm increases the approximation order N and repeats the first stage. Then, the second stage solves (13) as a least-squares problem. Besides, since the frequency response $f(s)$ is evaluated at several frequency points, Eq. (13) leads to an over-determined system of equations, where $f(s)$ and the poles a_n are known parameters, whereas c_n , d , and h are the unknowns.

The performance of the VF method depends on different factors, such as the initial poles estimate and the approximation order, as well as the adoption of a weighting function, which can improve the fitting results in a given frequency interval or minimize the relative fitting error rather than its absolute value. We refer the interested reader to [23], [24], [53] for more information about the VF algorithm and some of its further enhancements over time.

REFERENCES

- [1] L. G. Franquelo, J. Rodriguez, J. I. Leon, S. Kouro, R. Portillo, and M. A. M. Prats, "The age of multilevel converters arrives," *IEEE Industrial Electronics Magazine*, vol. 2, no. 2, pp. 28–39, 2008.
- [2] A. Lesnicar and R. Marquardt, "An innovative modular multilevel converter topology suitable for a wide power range," in *Power Tech Conference Proceedings, Bologna*, vol. 3. IEEE, 2003, pp. 6–10.
- [3] A. Dekka, B. Wu, R. L. Fuentes, M. Perez, and N. R. Zargari, "Evolution of topologies, modeling, control schemes, and applications of modular multilevel converters," *IEEE Journal of Emerging and Selected Topics in Power Electronics*, vol. 5, no. 4, pp. 1631–1656, 2017.

- [4] G. Bergna Diaz, J. A. Suul, and S. D'Arco, "Small-signal state-space modeling of modular multilevel converters for system stability analysis," in *2015 IEEE Energy Conversion Congress and Exposition (ECCE)*, 2015, pp. 5822–5829.
- [5] S. Debnath, J. Qin, B. Bahrani, M. Saeedifard, and P. Barbosa, "Operation, control, and applications of the modular multilevel converter: A review," *IEEE transactions on power electronics*, vol. 30, no. 1, pp. 37–53, 2014.
- [6] B. Bahrani, S. Debnath, and M. Saeedifard, "Circulating current suppression of the modular multilevel converter in a double-frequency rotating reference frame," *IEEE Transactions on Power Electronics*, vol. 31, no. 1, pp. 783–792, 2016.
- [7] J. Lyu, X. Zhang, X. Cai, and M. Molinas, "Harmonic state-space based small-signal impedance modeling of a modular multilevel converter with consideration of internal harmonic dynamics," *IEEE Transactions on Power Electronics*, vol. 34, no. 3, pp. 2134–2148, 2019.
- [8] S. Zhu, L. Qin, K. Liu, K. Ji, Y. Li, Q. Huai, X. Liao, and S. Yang, "Impedance modeling of modular multilevel converter in d-q and modified sequence domains," *IEEE Journal of Emerging and Selected Topics in Power Electronics*, pp. 1–1, 2020.
- [9] IEEE Harmonics Model and Simulation Task Force, "Modeling and simulation of the propagation of harmonics in electric power networks: Part I," *IEEE Transaction on Power Delivery*, vol. 11, no. 1, pp. 466–474, Jan. 1996.
- [10] T. Demiray, "Simulation of power system dynamics using dynamic phasor models," Ph.D. dissertation, ETH Zurich, 2008.
- [11] S. R. Deore, P. B. Darji, and A. M. Kulkarni, "Dynamic phasor modeling of modular multi-level converters," in *2012 IEEE 7th International Conference on Industrial and Information Systems (ICIIS)*. IEEE, 2012, pp. 1–6.
- [12] C. Guo, J. Yang, and C. Zhao, "Investigation of small-signal dynamics of modular multilevel converter under unbalanced grid conditions," *IEEE Transactions on Industrial Electronics*, vol. 66, no. 3, pp. 2269–2279, 2018.
- [13] O. C. Sakinci and J. Beerten, "Generalized dynamic phasor modeling of the mmc for small-signal stability analysis," *IEEE Transactions on Power Delivery*, vol. 34, no. 3, pp. 991–1000, 2019.
- [14] ——, "Equivalent multiple dq-frame model of the mmc using dynamic phasor theory in the $\alpha\beta z$ -frame," *IEEE Transactions on Power Delivery*, pp. 1–1, 2020.
- [15] S. Zhu, P. Liu, X. Liao, L. Qin, Q. Huai, Y. Xu, Y. Li, and F. Wang, "D-Q frame impedance modeling of modular multilevel converter and its application in high-frequency resonance analysis," *IEEE Transactions on Power Delivery*, pp. 1–1, 2020.
- [16] Y. Chen, L. Xu, A. Egea-Álvarez, B. Marshall, M. Rahman, and O. D. Adeuyi, "Mmc impedance modelling and interaction of converters in close proximity," *IEEE Journal of Emerging and Selected Topics in Power Electronics*, pp. 1–1, 2020.
- [17] Z. Xu, B. Li, S. Wang, S. Zhang, and D. Xu, "Generalized single-phase harmonic state space modeling of the modular multilevel converter with zero-sequence voltage compensation," *IEEE Transactions on Industrial Electronics*, vol. 66, no. 8, pp. 6416–6426, 2019.
- [18] H. Wu, X. Wang, and L. H. Kocewiak, "Impedance-based stability analysis of voltage-controlled MMCs feeding linear AC systems," *IEEE Journal of Emerging and Selected Topics in Power Electronics*, vol. 8, no. 4, pp. 4060–4074, 2020.
- [19] H. Wu and X. Wang, "Dynamic impact of zero-sequence circulating current on modular multilevel converters: Complex-valued ac impedance modeling and analysis," *IEEE Journal of Emerging and Selected Topics in Power Electronics*, vol. 8, no. 2, pp. 1947–1963, 2020.
- [20] M. Okumura, T. Sugawara, and H. Tanimoto, "An efficient small signal frequency analysis method of nonlinear circuits with two frequency excitations," *IEEE Transactions on Computer-Aided Design of Integrated Circuits and Systems*, vol. 9, no. 3, pp. 225–235, 1990.
- [21] F. Bizzarri, A. Brambilla, S. Grillo, and F. Milano, "Periodic small-signal analysis as a tool to build transient stability models of vsc-based devices," in *2016 Power Systems Computation Conference (PSCC)*, 2016, pp. 1–6.
- [22] F. Bizzarri, A. Brambilla, and L. Codicosa, "Shooting by a two-step galerkin method," *IEEE Transactions on Circuits and Systems I: Regular Papers*, vol. 66, no. 1, pp. 383–390, 2018.
- [23] B. Gustavsen, "Improving the pole relocating properties of vector fitting," *IEEE Transactions on Power Delivery*, vol. 21, no. 3, pp. 1587–1592, 2006.
- [24] B. Gustavsen and A. Semlyen, "Rational approximation of frequency domain responses by vector fitting," *IEEE Transactions on Power Delivery*, vol. 14, no. 3, pp. 1052–1061, 1999.
- [25] C. W. B4-57, *Guide for the Development of Models for HVDC Converters in a HVDC Grid*. CIGRÉ (WG Brochure), 2014.
- [26] A. Yazdani and R. Iravani, "A unified dynamic model and control for the voltage-sourced converter under unbalanced grid conditions," *IEEE Transactions on Power Delivery*, vol. 21, no. 3, pp. 1620–1629, 2006.
- [27] P. Kundur, *Power system stability and control*. New York: McGraw-Hill, 1994.
- [28] Q. Tu, Z. Xu, and L. Xu, "Reduced switching-frequency modulation and circulating current suppression for modular multilevel converters," *IEEE Transactions on Power Delivery*, vol. 26, no. 3, pp. 2009–2017, July 2011.
- [29] D. Guo, M. H. Rahman, G. P. Adam, L. Xu, A. Emhemed, G. Burt, and Y. Audichya, "Detailed quantitative comparison of half-bridge modular multilevel converter modelling methods," in *The 14th IET International Conference on AC and DC Power Transmission (ACDC 2018)*, 2018, pp. 1–8.
- [30] F. Gonzalez-Longatt and J. L. R. Torres, *Advanced Smart Grid Functionalities Based on PowerFactory*. Springer, 2018.
- [31] T. Roose, A. Lekic, M. M. Alam, and J. Beerten, "Stability analysis of high-frequency interactions between a converter and hvdc grid resonances," *IEEE Transactions on Power Delivery*, pp. 1–1, 2020.
- [32] U. M. Ascher and L. R. Petzold, *Computer methods for ordinary differential equations and differential-algebraic equations*. Siam, 1998, vol. 61.
- [33] A. Moawwad, E. F. El-Saadany, M. S. El Moursi, and M. Albadi, "Critical loading characterization for MTDC converters using trajectory sensitivity analysis," *IEEE Transactions on Power Delivery*, vol. 33, no. 4, pp. 1962–1972, 2018.
- [34] M. Günther and U. Feldmann, "The DAE-index in electric circuit simulation," *Mathematics and Computers in Simulation*, vol. 39, no. 5, pp. 573 – 582, 1995.
- [35] O. Nastov, R. Telichevesky, K. Kundert, and J. White, "Fundamentals of fast simulation algorithms for rf circuits," *Proceedings of the IEEE*, vol. 95, no. 3, pp. 600 –621, march 2007.
- [36] J. Aprille, T.J. and T. Trick, "Steady-state analysis of nonlinear circuits with periodic inputs," *Proceedings of the IEEE*, vol. 60, no. 1, pp. 108–114, Jan. 1972.
- [37] F. Bizzarri, A. Brambilla, and G. Storti Gajani, "Steady State Computation and Noise Analysis of Analog Mixed Signal Circuits," *IEEE Trans. Circuits Syst. I*, vol. 59, no. 3, pp. 541–554, Mar. 2012.
- [38] ——, "Extension of the variational equation to analog/digital circuits: numerical and experimental validation," *International Journal of Circuit Theory and Applications*, vol. 41, no. 7, pp. 743–752, 2013.
- [39] E. J. W. ter Maten, J. G. Fijnwandraat, C. Lin, and J. M. F. Peters, "Periodic AC and periodic noise in RF simulation for electronic circuit design," in *Modeling, Simulation, and Optimization of Integrated Circuits*, ser. ISNM International Series of Numerical Mathematics, K. Antreich, R. Bulirsch, A. Gilg, and P. Rentrop, Eds. Birkhäuser Basel, 2003, vol. 146, pp. 121–134.
- [40] F. Bizzarri, A. Brambilla, G. S. Gajani, and S. Banerjee, "Simulation of real world circuits: Extending conventional analysis methods to circuits described by heterogeneous languages," *IEEE Circuits and Systems Magazine*, vol. 14, no. 4, pp. 51–70, Fourthquarter 2014.
- [41] F. Bizzarri and A. Brambilla, "PAN and MPanSuite: Simulation vehicles towards the analysis and design of heterogeneous mixed electrical systems," in *NGCAS*. IEEE, 2017, pp. 1–4.
- [42] J. Beerten, S. D'Arco, and J. A. Suul, "Frequency-dependent cable modelling for small-signal stability analysis of vsc-hvdc systems," *IET Generation, Transmission Distribution*, vol. 10, no. 6, pp. 1370–1381, 2016.
- [43] H. Zong, C. Zhang, J. Lyu, X. Cai, M. Molinas, and F. Rao, "Generalized mimo sequence impedance modeling and stability analysis of mmc-hvdc with wind farm considering frequency couplings," *IEEE Access*, vol. 8, pp. 55 602–55 618, 2020.
- [44] T. Li, A. Gole, and C. Zhao, "Stablity of a modular multilevel converter based hvdc system considering dc side connection," in *12th IET International Conference on AC and DC Power Transmission (ACDC 2016)*, 2016, pp. 1–6.
- [45] K. Shinoda, A. Benchaib, J. Dai, and X. Guillaud, "Virtual capacitor control: Mitigation of dc voltage fluctuations in mmc-based hvdc systems," *IEEE Transactions on Power Delivery*, vol. 33, no. 1, pp. 455–465, 2018.
- [46] D. d. Giudice, F. Bizzarri, D. Linaro, and A. Brambilla, "Stability analysis of mmc/mtdc systems considering dc-link dynamics," in *2021 IEEE International Symposium on Circuits and Systems (ISCAS)*, 2021, pp. 1–5.
- [47] M. Farkas, *Periodic motions*. New York, NY, USA: Springer-Verlag New York, Inc., 1994.

- [48] R. Bellman, *Methods of nonlinear analysis*. New York, NY, USA: Academic Press, 1970.
- [49] F. Bizzarri, A. Brambilla, and G. Storti Gajani, "Periodic small signal analysis of a wide class of type-II phase locked loops through an exhaustive variational model," *Circuits and Systems I: Regular Papers, IEEE Transactions on*, vol. 59, pp. 2221–2231, 2012.
- [50] E. O. Kontis, T. A. Papadopoulos, A. I. Chrysochos, and G. K. Papagiannis, "Measurement-based dynamic load modeling using the vector fitting technique," *IEEE Transactions on Power Systems*, vol. 33, no. 1, pp. 338–351, 2018.
- [51] P. M. Ramos and F. M. Janeiro, "Vector fitting based automatic circuit identification," in *2016 IEEE International Instrumentation and Measurement Technology Conference Proceedings*, 2016, pp. 1–6.
- [52] L. Fan, Z. Miao, P. Koralewicz, S. Shah, and V. Gevorgian, "Identifying dq-domain admittance models of a 2.3-mva commercial grid-following inverter via frequency-domain and time-domain data," *IEEE Transactions on Energy Conversion*, pp. 1–1, 2020.
- [53] D. Deschrijver, M. Mrozwski, T. Dhaene, and D. De Zutter, "Macro-modeling of multiport systems using a fast implementation of the vector fitting method," *IEEE Microwave and Wireless Components Letters*, vol. 18, no. 6, pp. 383–385, 2008.



Federico Bizzarri (M'12–SM'14) was born in Genoa, Italy, in 1974. He received the Laurea (M.Sc.) five-year degree (*summa cum laude*) in electronic engineering and the Ph.D. degree in electrical engineering from the University of Genoa, Genoa, Italy, in 1998 and 2001, respectively. Since October 2018 he has been an associate professor at the Electronic and Information Department of the Politecnico di Milano, Milan, Italy. He is a research fellow of the Advanced Research Center on Electronic Systems for Information and Communication Technologies "E. De Castro" (ARCES), University of Bologna, Italy. He served as an Associate Editor of the *IEEE Transactions on Circuits and Systems — Part I* from 2012 to 2015 and he was awarded as one of the 2012–2013 Best Associate Editors of this journal.



Daniele Linaro received his MSc in Electronic Engineering from the University of Genoa (Italy) in 2007 and a PhD in Electrical Engineering from the same university in 2011. Since 2018, he is Assistant Professor in the Department of Electronics, Information Technology and Bioengineering at the Polytechnic of Milan. His main research interests are currently in the area of circuit theory and nonlinear dynamical systems, with applications to electronic oscillators and power systems and computational neuroscience, in particular biophysically-realistic single-cell models of neuronal cells.



Davide del Giudice was born in Milan, Italy, in July 1993. He received the B.S. degree and the M.S. degree (*cum laude*) in electrical engineering from Politecnico di Milano, Italy in 2015 and 2017 respectively. He is currently a PhD candidate at the department of Electronics, Information and Bioengineering of the Politecnico di Milano. His main research activities are related to simulation techniques specifically tailored to electric power systems characterised by a high penetration of renewable energy sources, such as HVDC systems.



Angelo Brambilla (M'16) received the Dr. Ing. degree in electronics engineering from the University of Pavia, Pavia, Italy, in 1986. He is full professor at the Dipartimento di Elettronica, Informazione e Bioingegneria, Politecnico di Milano, Milano, Italy, where he has been working in the areas of circuit analysis, simulation and modeling.